PERGAMON

Vision Research 43 (2003) 117–133

Vision Research

www.elsevier.com/locate/visres

A gain-control model relating nulling results to the duration of dynamic motion aftereffects

W.A. van de Grind *, M.J.M. Lankheet, R. Tao [1]

Department of Biology, Functional Neurobiology, Helmholtz Institute, Utrecht University, Padualaan 8, 3584 CH Utrecht, The Netherlands

Received 7 June 2002; received in revised form 18 September 2002

Abstract

Strength of the motion aftereffect (MAE) is most often quantified by its duration, a high-variance and rather 'subjective' measure. With the help of an automatic gain-control model we quantitatively relate nulling-thresholds, adaptation strength, direction discrimination threshold, and duration of the dynamic MAE (dMAE). This shows how the nulling threshold, a more objective two-alternative forced-choice measure, relates to the same system property as MAE-durations. Two psychophysical experiments to test the model use moving random-pixel-arrays with an adjustable luminance signal-to-noise ratio. We measure MAE-duration as a function of adaptation strength and compare the results to the model prediction. We then do the same for nulling-thresholds. Model predictions are strongly supported by the psychophysical findings. In a third experiment we test formulae coupling nulling threshold, MAE-duration, and direction-discrimination thresholds, by measuring these quantities as a function of speed. For the medium-to-high speed range of these experiments we found that nulling thresholds increase and dMAE-durations decrease about linearly, whereas direction discrimination thresholds increase exponentially with speed. The model description then suggests that the motion-gain decreases, while the noise-gain and model's threshold increase with speed.

Keywords: Aftereffect-nulling; Dynamic MAE; MAE-duration; Gain-control model

1. Introduction

A classical, or 'static' motion aftereffect (sMAE) is experienced if we look at a static test pattern after sufficiently prolonged adaptation to relatively slow motion (below about 12–20 deg/s). The effect has at least been known since Aristotle's time, but was first placed solidly on the map of vision research in the 19th and 20th century (reviews by Verstraten, 1996; Wade, 1994, 1998). From the start a major problem of MAE-research has been how one can best quantify the effect. Pantle (1998) summarises the various approaches and points out that the MAE-duration has been used most. Nulling (cancellation, compensation) of the sMAE has been recognised as an interesting alternative at least since the work of Cords and von Brücke (1907). However, it has been criticised on the grounds that it uses real motion to cancel paradoxical motion of the sMAE (Wade, 1994). This criticism does not hold for the dynamic MAE, or dMAE, an aftereffect experienced for medium to high adaptation speeds if a dynamic noise test pattern is used. The dMAE is perceptually indistinguishable from real motion (Blake & Hiris, 1993; Hiris & Blake, 1992). Here we assume that adaptation changes an automatic gain control in the motion system and that the nulling motion augments activity in the adapted channel to compensate for decreased gain. For such a gain-control model nulling methods have a reasonably straightforward interpretation. If a similar model holds for the sMAE a similar conclusion follows, but we specifically target the dMAE. The main goal of this paper is to show with the help of a gain-control model, how nulling thresholds of the dMAE relate to dMAE-durations and to validate the model-predictions in psychophysical measurements. This provides a general theoretical basis for the interpretation of MAE-phenomena and can be of great help in the design of experiments.

* Corresponding author. Address: Department of Comparative Physiology, Functional Neurobiology, Utrecht University, Padualaan 8, 3584 CH Utrecht, The Netherlands. Fax: +31-30-254-2219.

E-mail address: w.a.vandegrind@bio.uu.nl (W.A. van de Grind).

[1] On leave from the Eye Clinic of the Bao Tou Iron & Steel Company Hospital, Bao Tou, Inner Mongolia, People's Republic of China.

0042-6989/03/$ - see front matter
PII: S0042-6989(02)00495-9

We will argue more extensively in the discussion that our measurements select a 'high-speed' motion channel that is responsible for the dMAE. The present results are therefore not necessarily relevant for the sMAE. This point was made before by Blake and Hiris (1993) who developed a nulling method that is in principle similar to ours. The main difference is that they used sparse random dot patterns with a coherence measure based on the percentage of dots moving in the same direction amidst dots moving in random directions. We use moving random-pixel arrays (RPAs, moving Julesz-patterns) with variable amounts of first-order (luminance-based) motion information, quantified by the luminance signal-to-noise ratio (LSNR). The LSNR-value of a test motion pattern that cancels the dMAE will be called the nulling threshold. It represents the amount of motion energy necessary to null the MAE relative to non-drifting noise energy. Compared to moving sinewave gratings our stimulus has the advantage that it does not suffer from aliasing problems. For example, a sinewave pattern stepping an integer number of periods per frame cannot be discriminated from a non-moving sinewave pattern, whereas any step size (smaller than the screen-size) per frame of an RPA defines and looks like motion. Compared to sparse random dot patterns a moving RPA has the advantage that it maximises the number of stimulated motion sensors per unit area of the visual field and thus gives a maximum MAE.

The large number of options for adaptation and test stimuli has led to many papers on the MAE that are difficult to relate to each other or to work on motion perception in general. It seems important therefore to try to develop theories and models that can be used as effective tools of thought to tie together the various phenomena of the MAEs and of motion detection. As a modest contribution to this goal we develop an automatic gain-control stage for a MAE network model developed by Grunewald (1996). The network model can explain several crucial results and correctly predicted a new phenomenon (Grunewald & Lankheet, 1996). One strength of the network model is that it explains the finding (Verstraten, Fredericksen, & van de Grind, 1994) that adaptation to two motion patterns at the same time and place (so-called 'bi-vectorial' transparent motion) normally leads to univectorial MAEs. It also explains the one exception where adaptation to opponent motion can, under favourable conditions, lead to an orthogonal transparent MAE (Grunewald & Lankheet, 1996). Moreover, the Grunewald–Lankheet model encompasses previous models like the ratio-model (Moulden & Mather, 1978; Sutherland, 1961) and 'distribution-shift' model (Mather, 1980; Mather & Harris, 1998).

An automatic gain-control mechanism, the ultimate cause of MAEs, will be described in some detail, so that it can be used to quantitatively explain (describe) the psychophysical findings. Such a gain control stage is assumed to be present in each direction-specific channel of the Grunewald-network. It is necessary to add one generalisation to the network model, so as to provisionally extend it in the speed dimension. Moreover, and most importantly, we will assume that the model is also valid (albeit with different parameters) for the more recently described dMAE, the topic of this paper. We have reason to believe that the dMAE and the sMAE are generated in separate parallel networks (van de Grind, van Hof, van der Smagt, & Verstraten, 2001; van der Smagt, Verstraten, & van de Grind, 1999), possibly in different brain regions. We assume that these networks have a highly similar structure, dictated by the computational tasks and their possible neuronal implementations, but differ in several parameter values.

Fig. 1 illustrates the Grunewald-network that will be used as our starting point. For the sake of simplicity we have drawn only 12 motion sensors in the input layer, one for each clock-direction. They are assumed to represent direction-selective cells in $V1$. Either in $V1$ at the output or in the next station (e.g. $V5$) at the input we find an automatic gain-control unit (circle crossed by oblique line in Fig. 1). The model comprises three layers even though these might physiologically only represent two cell-layers. The directional tuning curve of the sensors is a Gaussian with a half-width of, say, 30°–45°. We have only drawn the divergence of signals from the 6 o'clock channel's gain-unit to the integrator layer, but

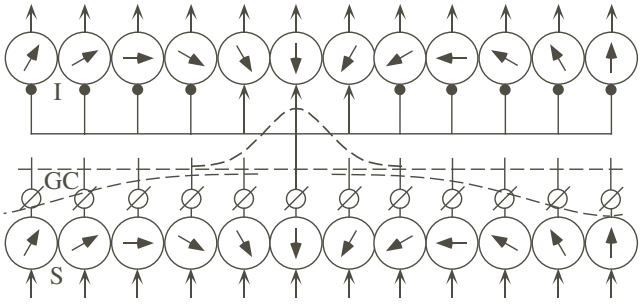

Fig. 1. Schematic representation of the Grunewald MAE network model. The lower layer (S) is the sensor layer and consists of direction selective speed-tuned sensors, possibly $V1$ neurons. They are each followed by an automatic gain control stage (circle crossed by an oblique line), the main topic of the present paper. Whereas the input sensitivity is represented by a velocity-dependent fixed motion-gain factor $g_m(V)$, the gain control has an adaptation-dependent gain $g(V,t)$. Arrows in the units of the S- and I-layer symbolise optimal tuning directions. Each direction specific sensor projects via its gain stage onto a range of 'similar-direction' I-cells (excitatory connections) and to a wider range of 'unsimilar-direction' cells (inhibitory connections). 'Unsimilar-direction' refers to a range of directions around and similar to the opponent direction. Here we only included connections from the six o'clock direction sensor to the integrator cell layer, but every sensor has the same type of projection to the I-layer centered around its own preference (excitatory, arrows) and opponent directions (inhibitory, closed circles). An explanation of the network actions is given in the text.

all sensors have a similar mapping upon the integrator layer. This mapping consists of a relatively narrow spread of excitation, making the direction tuning curve of integrator units about 90° wide (as in $V5$-units in the monkey), and a very broad spread of inhibition, centered on the unit of opposite direction-selectivity. In the example of Fig. 1 this is the 12 o'clock unit. The spread of inhibition is also Gaussian.

The gain-units are assumed to have a resting gain of 1, which goes down on adaptation (never reaching 0 of course) and recovers exponentially after adaptation. Such an automatic gain control is easy to construct from a leaky integrator with a relatively long time constant, as will be explained below in connection with Fig. 3. The basic idea of the network model is that a lowered gain in, say, the 6 o'clock channel will give it a lower output during testing than the 12 o'clock channel, due to the decrease of the latter channel's inhibition from the 6 o'clock channel (disinhibition). During testing the 12 o'clock channel will therefore be the most active of all. In case of bivectorial adaptation, the wide spread of inhibition will ensure a fusion of aftereffects into one single direction. We refer to Grunewald and Lankheet (1996) for further details on this aspect of the model. Note that the inhibition pattern becomes manifest as soon as all the direction-channels are stimulated, during the MAE-test, but not if thresholds are measured for a single motion direction. For example, the threshold of

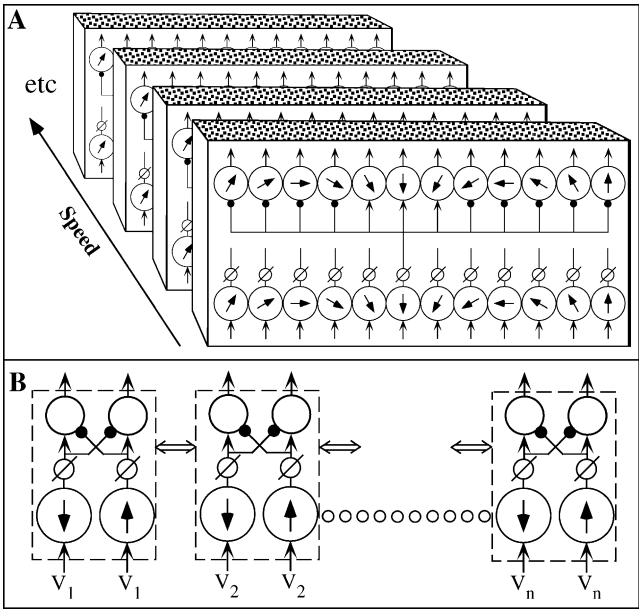

Fig. 2. In A we symbolise that a Grunewald network (Fig. 1) might exist for each of a range of speeds. The gain controls of any of the networks might get input from other speed-tuned networks as well, but we will address one speed at a time, so that these interactions in the speed-direction play no role. We will only consider opponent-direction channel-pairs from each speed layer, as indicated in B. The automatic gain control circuits (small circles, each crossed by an oblique line) are specified in Fig. 3.

the adapted channel is increased, but that of the opponent channel is unchanged. The model was originally designed to explain phenomena of the sMAE. Here we assume that a similar network is responsible for the dMAE.

The Grunewald network is designed for all directions, but only one speed. The simplest extension in the speed-dimension is to postulate that there is such a network for each of a large number of speeds, as symbolised in Fig. 2A. Because the MAE-duration is speed-dependent, every separate speed-specific Grunewald-network might have its own time-constant of adaptation and recovery of its gain. Obviously the speed-specific networks must somehow interact, spread their excitation and/or inhibition across neighbours or to more distant regions. In other words: the gain-units must have a receptive and projective field structure in the speed dimension as well as in the direction dimension. Fig. 2B illustrates which part of the complex network of Fig. 2A will be relevant in the present analysis. Every speed-specific network is only represented by two opponent direction-channels. The interactions between speed-specific networks (double arrows in Fig. 2B) are neglected, since we only used one speed at a time in our experiments. Here we will concentrate on the automatic gain controls, and quantify their influence on the dMAE.

Suppose one would want to null the MAE in a Grunewald network or in the degenerate version used in this paper (Fig. 2B). What has to be done is in principle rather simple: send an extra signal through the adapted channel, such that its output equals that of the other channels during testing. This will eliminate the disinhibition effect on channels around the opponent direction as well as compensate for the lower output of the adapted channel. The model predicts that perfect nulling should be possible by adding a weak stimulus of the same kind (direction etc.) as the adaptation stimulus. Due to the neglected complexities of interactions in the speed dimension one cannot expect this nulling to be perfect for long. Eventually the focus of gain-imbalance might drift towards other (less-adapted) speed-specific layers, e.g. because they have longer recovery time-constants. Therefore we concentrate on nulling immediately after adaptation, while the gain is still maximally modulated in the targeted speed-specific network.

The following section describes our gain-control model in some detail and shows how nulling threshold and MAE-duration are related to adaptation strength. We also derive a relation between MAE-duration and nulling-threshold. Our next aim is to test the model predictions in three psychophysical experiments. To do so, stimulus variables have to be mapped onto model variables. Before we can discuss our solution to this mapping-problem we need to describe the stimuli. After developing model relations and the basic plan for three psychophysical experiments in the next section, we will

therefore describe the stimuli and their basic parameters (methods), before translating the model formulae into psychophysical predictions in the introduction to the experiments. To keep the model and psychophysical domains clearly separated we will use the following convention. *Signals* in the model domain are denoted with an x plus index (e.g. $x_0 =$ the nulling signal, $x_A =$ adaptation signal), whereas the psychophysical measure of *signal strength* is always an LSNR-value, denoted as S with a corresponding index (e.g. S_0 for nulling or S_A for adaptation LSNR-values).

2. Gain-control model

Fig. 3 presents the gain-control model that will be used in this paper. It has a feedforward-divisive (FFD-) structure. We have studied three alternative models as well. For example, one can make the gain g (see Fig. 3) equal to $1 - u$, to obtain a feedforward multiplicative (FFM-) version. If the leaky integrator is connected to the output rather than input one gets a feedback-divisive (FBD-) and feedback-multiplicative (FBM-) version, respectively. Some formulae (e.g. formula (3) below) can be written in such a form that they hold for all four models. In many respects the model-choice is not very critical so that we can view the chosen FFD-version as a generic model, representing a class of models. Yet, except for formula (3) below, the other formulae are specific for the FFD-model, which we used to interpret our psychophysical results.

It is possible to choose the signal-range at the model input relatively arbitrarily, because it only influences two linear scaling factors (g_m, the motion signal gain, and g_n, the noise signal gain: Fig. 3) in the mapping function that translates psychophysical quantities into model quantities. We chose the input range from 0 to 10.

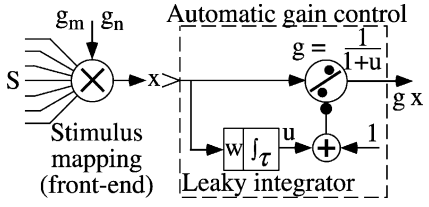

Fig. 3. Schematic diagram of an automatic gain-control system of the feedforward divisive (FFD-) type, as described in the text. An ensemble of motion sensors of equal speed-tuning converge at the input and are weighted by the overall input motion-signal gain g_m. This gain depends upon number and sensitivity of the converging sensors. Noise has a different mapping gain g_n. In the gain-control proper (box of interrupted lines) a leaky-integrator with input weight w and time constant τ determines the adapted gain. Its output signal u is used to control gain factor $g = 1/(1 + u)$. Weight w has to be small enough to ensure that g will not approach zero. In fact g should probably never be lowered more than 0.1–0.5 below its resting value of 1. There are no psychophysical indications that the gain can get substantially smaller. With this choice we can then fix the value of w, the input weight of the leaky integrator (Fig. 3). For a constant maximum input $x = 10$, gain g in Fig. 3 would adapt to a minimum value of $(1 + 10w)^{-1}$, so it is advisable to choose a relatively small value for w. We chose $w = 0.05$, so that the minimum value of g is 2/3 of the unadapted value of 1. There is no direct information on the maximum gain factor decrease after prolonged adaptation, but it is certainly not extreme. For example, Raymond (1993) studied the increase of a motion coherence threshold after adaptation, and found an increase from 14.3% to 62.8% for a speed of 1.68 deg/s. It is not immediately obvious how this can be translated in model-terms, especially because the test only consisted of a single motion step of a sparse dot stimulus. But it illustrates that the threshold increase is relatively modest. In accordance with her findings our model shows no threshold-increase for directions that differ (sufficiently) from the adaptation direction. After fixing w, our gain-control model only has two free parameters, time constant τ and a threshold criterion θ (see below). In addition, the front-end mapping symbolised in Fig. 3 has two free parameters, g_m, the motion signal gain, and a parameter that characterises the effectiveness of test noise at the gain-control (noise gain g_n, see later). One aim of the paper is to show how these four parameters can be determined unambiguously from psychophysical measurements.

To facilitate the derivation of predictions for the three psychophysical experiments in the next sections, we first discuss a few general properties and explain the notational conventions. In the non-adapted case, gain g (defined in Fig. 3) will be 1, so the signal going to the integrator units and beyond then equals input signal x. If this signal has to surpass some fixed threshold θ to be perceived, the threshold input signal x_d will equal θ. We will use this equality in the analysis of experiment 3. During adaptation the stimulus causes some constant neural signal x_A at the gain-control input, so the leaky integrator (an RC-integrator) will charge. The leaky integrator has a time constant τ and a small input weighting factor w ($w = 0.05$), so its output u at time t after the start of adaptation (at $t = 0$) will be:

$$u(t) = wx_A(1 - e^{-t/\tau}) = F(t)x_A \quad (1)$$

where index A refers to the adaptation phase and $F(t)$ is defined as $F(t) = w(1 - e^{-t/\tau})$. Let us use a star to characterise the various quantities at the end of a complete adaptation period of t^* s. Thus u^* denotes the charge of the leaky integrator at the end of adaptation, just before testing, and is given by formula (1) with $t = t^*$, so we have

$$u^* = F^* x_A \quad (2a)$$

$$F^* = w(1 - e^{-t^*/\tau}) \quad (2b)$$

where F^* is constant for a constant adaptation duration and time constant. F^* can change with speed, because we assume that τ can change with speed-tuning of the targeted network. If the adaptation period t^* lasts n times τ s and n is large enough, we can regard F^* as equal to w and constant at any speed. (For example, for $n = 4$ we have $F^* = 0.982w$, for $n = 5$ $F^* = 0.993w$, etc.)

Input signals to the automatic gain control itself will always be denoted as x, with an index to show their kind or size. For example, x_A is the adaptation value of x, x_t is the test value of x (during testing of the MAE), x_0 is the nulling motion signal at the gain-control's input, and x_d is the threshold value of x. (We used d from the dutch 'drempel', meaning 'threshold', because the t was already used for 'test'.) Later we will use exactly the same convention for stimulus values in the psychophysical domain. They are all luminance signal-to-noise ratios, the value of which is denoted as S, and we will use exactly the same indices to indicate their kind, such as S_A for the adaptation strength.

2.1. MAE-durations and experiment 1

Let us first present a formula for the MAE-duration. During recovery (testing) u leaks exponentially (time constant τ) from starting value u^* towards an end value determined by the test stimulation. For a fixed time constant and test stimulus the duration of this recovery phase is mainly determined by u^*. To calculate the MAE-duration one needs a MAE detection criterion. We assume that the MAE is visible as long as the difference between the opponent channel's output and the adapted channel's output exceeds θ. All four versions of an automatic gain-control model mentioned above lead to a logarithmic relation between MAE-duration T and u^*, which can be written (Appendix A) as

$$T = \tau \,\mathrm{Ln}(bu^*/\theta) \tag{3}$$

Factor b is a different expression for each of the models (and sometimes a small additive term has to be added to the Ln-function's argument as well). For the FFD-model of Fig. 3 we will use the following approximate result (Appendix A):

$$b \approx (x_t - \theta)/(1 + wx_t)^{-2} \tag{4}$$

where x_t is the excitation value of the noise test. As explained in the appendix this approximation depends on the values of the various model variables, and is certainly not universally valid, but an exact formula can always be calculated if necessary. For a constant test signal in the psychophysical domain, the value of x_t might be different for gain-controls in different speed-tuned channels. Thus b can be treated as a constant only for a constant test stimulus and a constant adaptation speed. If these conditions are met θ will also be constant and formula (3) predicts a simple linear relation between T and $\mathrm{Ln}(u^*)$. This also entails a similar relation of T and the Ln of adaptation strength x_A because formula (2a) in (3) gives

$$T = \tau \,\mathrm{Ln}\{(bF^*/\theta)x_A\} \tag{5}$$

Relation (5) will be tested in the first psychophysical experiment, in which we measure dMAE-duration T as a function of adaptation strength for a fixed speed (so that b, τ, F^* and θ are constant). The experiment will be done for three speeds in a range where one can expect a strong dMAE, viz. 6, 12, and 18 deg/s, and we will use moving random pixel arrays with a variable LSNR.

2.2. Nulling thresholds and experiment 2

What happens during nulling? In that case we selectively apply an extra input signal x_0 to the adapted direction-channel, whereas the test signal (noise) stimulates all direction-channels equally. Unadapted channels, such as the opponent of the adapted direction, only carry signal x_t^0, where x_t^0 is the excitation of all direction-tuned gain-controls for the chosen velocity by the dynamic noise of the test pattern. That such a noise-excitation of motion channels must exist follows from the fact that no dMAE is seen in darkness or on a static test pattern, dynamic noise is *required* to see a dMAE. Note that x_t^0 is not the same test stimulus as used in a duration dMAE-measurement with a standard noise test x_t. During nulling experiments the noise (=test) component and the nulling-signal component are both present and usually a decrease of the nulling signal automatically means an increase of the noise component and vice versa. In any case, this is the principle we used, as will be explained in the methods section. The maximum value of x_t^0 is reached when no motion signal is present, so $\mathrm{Max}[x_t^0]$ equals x_t as we use it in a MAE-duration test. In the adapted channel $g \neq 1$ so the signal carried there is the sum of nulling and test signals multiplied by gain g. We use a Quest method to null the dMAE (see Section 3), which means that we estimate the point of equality of signals carried by the adapted channel and its opponent. In other words nulling means that

$$g(x_0 + x_t^0) = x_t^0$$

or, if we null briefly and immediately after (re-)adaptation, while the situation is still about equal to that at $t = t^*$:

$$1/g^* = 1 + x_0/x_t^0$$

By definition (Fig. 3) $g = (1 + u)^{-1}$, so that $1/g^* = 1 + u^*$, from which we see with the previous relation that:

$$x_0/x_t^0 = u^* \tag{6a}$$

or with (2a)

$$x_0/x_t^0 = F^* x_A \tag{6b}$$

Of practical importance in this derivation is the assumption that the leaky integrator does not 'leak' significantly during brief testing periods and that the nulling stimulus does not change the integrator's charge significantly.

In psychophysical experiment 2 we test model prediction (6b), which is independent from prediction (5), tested in the first experiment. The idea is to measure nulling threshold S_0, an LSNR-value, in between re-adaptations, and for a constant speed. This should ensure that F^* can be regarded as constant, so that the nulling threshold has a simple relation with adaptation strength.

2.3. Relation between MAE-durations and nulling thresholds

According to (6a) nulling thresholds are directly related to u^*, the leaky integrator's charge at the end of adaptation, and according to (3) T is related to the Log of u^*. Formulae (6a) can be inserted in (3) to show a (logarithmic) relation between results of duration measurements and nulling measurements:

$$T = \tau \mathrm{Ln}\{(b/\theta)(x_0/x_t^0)\} \tag{7}$$

Formulae (3) and (6) show explicitly that both psychophysical methods (nulling and duration measurements) probe u^*, the 'hidden' variable that determines aftereffect strength. This conclusion from the above model analysis is of practical and theoretical importance, because it ties together two methodologies that have so far been used independently, and it even shows how their results can be translated into each other (formula (7)). We have found no earlier attempts in the literature to do so.

2.4. Speed-dependencies: experiment 3

If we take a closer look at (7) we see that there are two terms, of which the first one describes the influence of test noise (and the model's threshold) on MAE-duration. This term is certainly speed-dependent, because we know that the low speed channels do not react to random-noise test-patterns. Provided τ is known the term b/θ can be determined from measurements of both MAE-duration and nulling-thresholds. If we also want to know b in absolute terms it is necessary to measure unadapted threshold values as well as to estimate θ $(= x_d)$. These considerations led to the design of experiment 3 in which we measure MAE-duration, nulling-threshold and direction-discrimination threshold, all as a function of speed.

3. Methods

3.1. The nulling- and detection-threshold stimuli

Moving random-pixel arrays (RPAs) of 256×256 pixels are generated by a custom-built hardware device, controlled by a Macintosh computer. The patterns are presented on a CRT-display (Electrohome model EVM-1200, P4 phosphor) at a frame rate of 90 Hz. We used the LSNR-method developed by van Doorn and Koenderink (1982a,b). On every frame of the 'signal' RPA a new noise RPA is added pixel-by-pixel in such a way that the rms (root-mean-square-) contrast of the sum $C = \sqrt{(C_m^2 + C_n^2)}$ is kept constant at 0.7 or 70%. C_m is the rms contrast of the coherently moving RPA and C_n of the added dynamic noise patterns. The ratio of signal-pattern to noise-pattern variances is changed according to the subject's responses. It is the LSNR-value $S = C_m^2/C_n^2$. A hardware look-up table is used to set the luminance of each pixel accordingly. The patterns step i pixels between subsequent frames, so that the speed is i pixels per frame (ppf). At a viewing distance of 2 m, as used in these experiments, the pixel-size on the screen was 1 arcmin, so that a speed of 1 ppf corresponds at 90 frames/s to $V = 1.5$ deg/s.

3.2. Adaptation and nulling

In experiments 1 and 2 the adaptation LSNR-value is varied from 0.05 to 400. In experiment 3 the adaptation stimulus is a moving RPA of a high and constant LSNR-value (400). In all cases the average luminance is 50 cd/m^2. Nulling stimuli have the same average luminance and the same spatio-temporal properties as adaptation stimuli, but differ in LSNR-setting. Both adaptation and nulling stimuli have a constant rms-contrast of 0.7 (70%). After a pre-adaptation of 15 s, a periodic sequence starts of 5 s top-up adaptation and 0.5 s testing (nulling). Subjects have to indicate the perceived direction of motion during test-intervals in a two-alternative forced-choice task. If adaptation motion is to the right and the MAE therefore to the left, a nulling-stimulus of low LSNR in the test-interval moves to the right. If the MAE is stronger motion to the left is seen, if the nulling stimulus is stronger motion to the right is seen. A Quest staircase procedure (Watson & Pelli, 1983) was used to estimate the 50% point in 30 test-intervals. The LSNR-value of this 50% point is the nulling-threshold, S_0, at the chosen speed.

3.3. Direction-discrimination threshold and MAE-duration measurements

To measure the (unadapted) direction-discrimination thresholds S_d in experiment 3 we also use a Quest-staircase procedure with a two-alternative forced-choice

method, but now the stimulus moves randomly to the left or right. A Quest procedure varies the LSNR in such a way that the staircase converges on 85% correct answers. The staircase consisted of 50 trials. Presentation duration of the trials was 0.5 s and the subject started the next trial by pressing a key.

MAE-durations were measured in both the first and third experiment after 30 s adaptation at the chosen speed. The same step rates and step sizes were used as in the nulling experiments, to ensure compatibility. Intervals between the end of adaptation and the observer's key press, which indicated the end of a MAE, were timed by the computer.

3.4. Observers, viewing and presentation conditions

Subjects were seated at the end of a dark tunnel in which the monitor was placed at 2 m from the nodal point of their right eye. The left eye was covered. Chin support and forehead rest stabilised the head in space. The experienced observers were instructed to fixate a cross, consisting of two perpendicular lines of 4 pixels length, in the center of the screen. Stimuli were presented in a circular aperture with a diameter of 256 pixels (4.27 deg) in an otherwise dark environment. The computer controlled the Quest staircase, stimulus parameters and warning sounds, using software designed and written by one of the authors (ML). For duration measurements we used software written by R.E. Fredericksen, who also wrote interface software driving the IEEE-bus of our custom-built hardware stimulus generator (noise image machine or NIM). The three authors served as subjects in all experiments.

4. Psychophysical experiments

4.1. General introduction: the mapping of LSNR-values onto model signals

To test the model predictions psychophysically, we now need to map psychophysical stimulus strength S (a LSNR) onto the model signals x. From previous experiences with our LSNR-method we know that fixed S-increments, ΔS, make a lot of perceptual difference for small S values, but less and less for increasing S-values. This means that the function, mapping S-values on x-values should show a saturation-type non-linearity. It should smoothly converge on a fixed upper limit, because one cannot perceptually discriminate different stimuli with S-values above about 400–1000. At the other end of the scale the curve should be steep and go through zero for $S = 0$. This is a logical requirement, because $S = 0$ means that there is no motion-signal contrast at all, that is, $C_m = 0$ (For definitions of C_m, C_n, C, and their relations, see Section 3). Taken together this suggests that x should be proportional to C_m^2/C^2, which measures the ratio of signal-variance to the overall variance of signal-plus-noise, and is therefore a principled choice. This ratio is zero for zero signal contrast, increases steeply in the low signal-variance range, and converges in saturation-like manner on an upper limit, where all the variance (squared contrast) of the stimuli is signal variance. With the formulae of the methods section C_m^2/C^2 can be rewritten in terms of S, leading to the proposed mapping formula:

$$x = g_m S/(1 + S) \tag{8a}$$

This is not only a principled choice, it also conforms to Weber's law and to Naka–Rushton compression formulae as often used in the electrophysiological literature (for a review see van de Grind, Grüsser, & Lunkenheimer, 1973).

Formula (8a) can only be used for motion stimuli, not to transform dynamic test noise strength into a model excitation value x_t. There is a simple reasoning that makes it possible to include noise-sensitivity, albeit at the cost of an extra gain-variable g_n, the 'noise-gain'. During nulling the noise component's strength is the inverse of the motion signal strength, or S_0^{-1}, the noise-to-signal ratio. Therefore we can use formula (8a) with S_0 replaced by S_0^{-1} to express the noise strength. However, we do not know a priori whether noise gain correlates with motion gain. In fact this is unlikely, because low-speed sensors do not react to dynamic noise, despite their motion sensitivity. It is therefore necessary to include a different mapping gain factor, which leads to:

$$x_t^0 = g_n S_0^{-1}/(1 + S_0^{-1}) \tag{8b}$$

The maximum value of this term is reached when $S_0 \to 0$, in which case we find

$$x_t = g_n \tag{8c}$$

This is the noise strength used during MAE-duration measurements.

4.1.1. Experiment 1: influence of adaptation strength on the MAE-duration

Formula (8a) can be inserted in formulae (5) to obtain a model prediction in a form suitable for psychophysical testing:

$$T = c_1 + 2.3\tau \,\mathrm{Log}\{S_A/(1 + S_A)\} \tag{9a}$$

Note the switch from Ln to Log, which facilitates curve fitting. In this formula

$$c_1 = 2.3\tau \,\mathrm{Log}(bF^* g_m/\theta) \tag{9b}$$

where b, F^*, g_m, and θ were discussed in the model section. The purpose of experiment 1 is to measure T as a function of adaptation strength S_A and test how well model prediction (9a) describes the psychophysical results. If it does, we view this as support for both the presented gain-control model and mapping assumption

(8a). We will measure T at a fixed speed and fixed adaptation duration, so that c_1 and τ are constants that can be used to fit formula (9a) to the data. By measuring the relation at different speeds we get an impression of the change of τ with speed. The factors making up c_1 will be studied as a function of speed in the third experiment.

Fig. 4 presents results of an experiment with three observers in which dMAE-duration was measured as a function of LSNR-value S_A of the adaptation stimulus. For each observer one example is given in the graphs of a fitted curve and of the standard deviations as a function of adaptation strength. The complete results of fitting predicted relation (9a) to the data can be found in Table 1. The fourth panel of Fig. 4 presents averages across subjects per speed (symbols). Because the averaged results for the different speeds are so similar we also calculated the average and standard deviation of the whole data set per S_A-setting. The vertical bars in the fourth panel show the standard deviations, and the smooth curve is a fit of formula (9a) to the average data, with coefficients $c_1 = 8.186$, $\tau = 2.633$, and correlation coefficient $r^2 = 0.993$. This is a superb fit. For each speed the MAE-duration was measured six times per

Table 1
Coefficient-values c_1 and τ of least-square fits of formula 9a to the psychophysical results of experiment 1 for three observers and three speeds (Fig. 4). The last column gives the correlation coefficients

Subject	Speed (ppf)	c_1	τ	r^2
ML	4	8.859	1.968	0.793
	8	8.531	3.023	0.926
	12	7.394	2.541	0.976
WG	4	7.884	2.360	0.893
	8	6.723	2.520	0.936
	12	6.661	2.787	0.867
RT	4	6.893	1.786	0.825
	8	9.584	2.700	0.881
	12	10.897	3.134	0.921

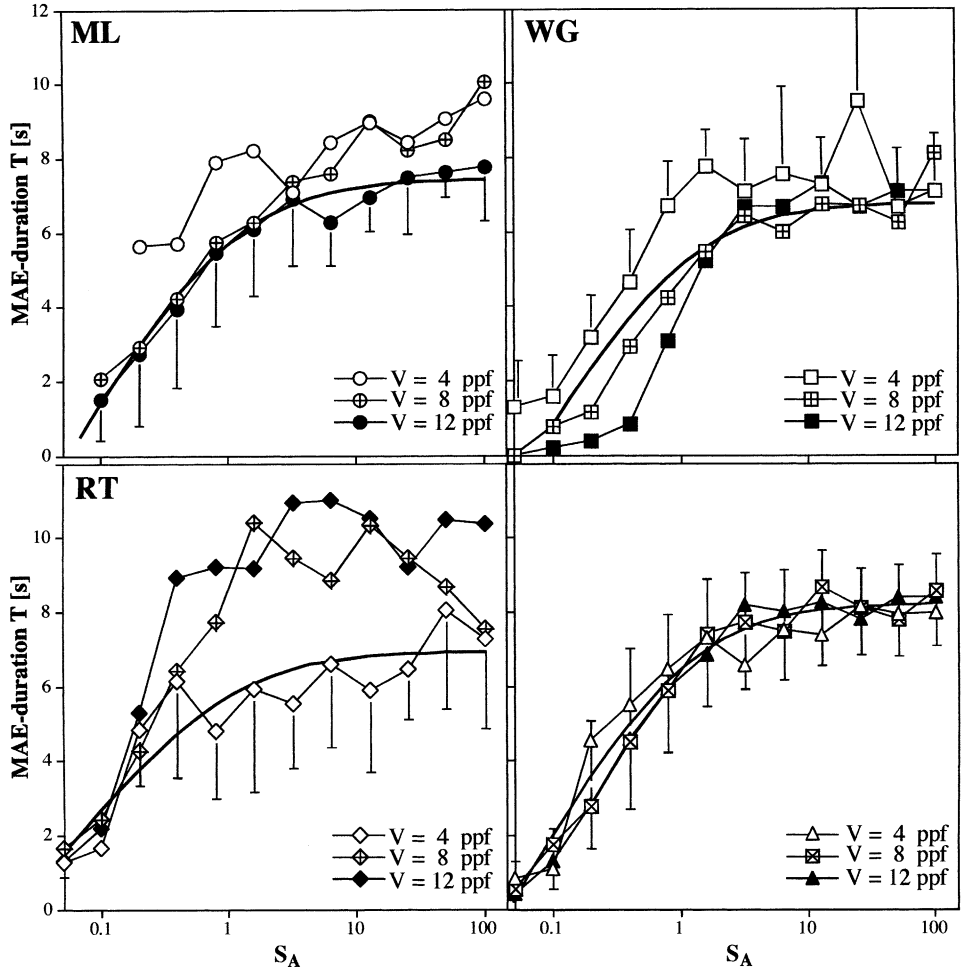

Fig. 4. Results of the first experiment: dMAE-duration T (ordinate) as a function of adaptation strength S_A (abscissa). Circles: subject ML, squares: subject WG, diamonds: subject RT. Open symbols: data for 4 ppf (6 deg/s), crossed symbols: data for 8 ppf (12 deg/s), filled symbols: data for 12 ppf (16 deg/s). The fourth panel (lower right) presents averages across subjects for each speed separately, and the standard deviations calculated for the overall average across subjects and speeds (54 duration values per S_A-value). The continuous curve in this panel is the best fit of formula (9) of the text to the overall average data.

subject and per S_A-value, so the grand average and its standard deviation were calculated from 54 duration measures per S_A-setting. Average, standard deviation, and fitted curve in the fourth panel give a good impression of the general relation between T and S_A. The data for individual subjects in the other panels show that the speed-tuning of MAE-durations varies between subjects, as has been reported before (e.g. van de Grind et al., 2001). For example, subject RT has shorter MAE-durations for low speeds and longer durations for high speeds compared to the other two subjects, indicating a speed-tuning curve shifted somewhat towards higher speeds.

The goal of this experiment was to test prediction (9a) of the model. The examples of data-fitting in Fig. 4 (one per panel) show that relation (9a) fits the data very well and we found that it describes the grand average of all data superbly. The parameters c_1 and τ as well as correlation coefficient r^2 of the fit are given in Table 1 for each of the subjects and speeds. Table 1 shows that the time constants for dMAEs vary between 1.8 and 3.1 s for the speeds and subjects of this experiment.

The relative standard deviation of these duration-measurements ranged from an average value of 24% at medium to high T-values to 35% at low T-values. The values of individual relative standard deviations ranged from 6% to 55%, except for two peak values above 100%. This reflects that MAE-duration data are always rather noisy. In this connection it must be emphasized that the present variances are relatively modest due to the fact that our subjects are highly trained. With untrained subjects we routinely get substantially higher variances of repeated measures. For this reason the MAE-duration is not a very attractive quantifier of the state of motion adaptation, especially not if untrained subjects are used in an experiment.

The experience of our observers was that it is relatively hard to judge the MAE-duration at low S_A-values, because it is very brief. Any hesitation in signalling the end of a MAE expresses itself as a major relative extension of the duration. Also it is sometimes hard to judge whether there was a MAE or none at all in these cases. Therefore durations tend to be over-estimated at the low end of the curve. Once you become certain of the MAE at somewhat higher S_A-values they already last some 3–5 s and subjectively nothing much changes then with increasing S_A. The curve for $V = 4$ ppf of subject ML (upper left panel in Fig. 4) illustrates this problem quite clearly. We found that it is useful to excercise reporting MAE-durations for very weak adaptation stimuli promptly in order to get short and consistent durations. One has to overcome the tendency of scrutinising the display for some remaining local movement and of hesitating in deciding that no MAE is seen (anymore). This is more of a decision than a perceptual problem. Despite this problem at very low adaptation levels, we think the data are described so well by formula (9a), that the model and mapping formula (8) are clearly supported by these psychophysical results.

4.1.2. Experiment 2: influence of adaptation strength on the nulling threshold

With formulae (8a) and (8b) the left-hand side of formula (6) reduces to $g_m S_0/g_n$, and after transforming the right-hand side with formula (8a) we find

$$S_0 = F^* g_n S_A/(1 + S_A) \tag{10a}$$

Because the effective adaptation duration is long enough in these experiments we can replace F^* by $w = 0.05$. For convenience of curve-fitting formula (10a) can then be written as

$$S_0 = c_2 + 0.05 g_n[S_A/(1 + S_A)] \tag{10b}$$

where fitting constant c_2 should have values around zero.

Purpose of the second experiment is to measure nulling-threshold S_0 as a function of adaptation strength S_A and to test how well model prediction (10b) describes the psychophysical results. This test is independent of the previous one (experiment 1), so if formula (10b) describes the results well this is additional support for the model and mapping assumption.

Fig. 5 shows how nulling threshold S_0 depends on the adaptation strength S_A for the three subjects of this experiment (panels labelled ML, WG and RT). Nulling-thresholds were measured three times for every condition and each measurement consisted of 30 trials. Three different speeds were used (4, 8 and 12 ppf, that is 6, 12 and 18 deg/s), as indicated in Fig. 5. The smooth curves are least-squares fits of function (10b) to the data.

Fig. 5 shows that the fit of model prediction (10b) is excellent for each of the three speeds and each of the three subjects. Coefficients of the least-squares fits are summarised in Table 2. Correlation coefficients r^2 range from 0.931 to 0.991 for the nine curves, so we can conclude that this experiment provides a very strong confirmation of the model predictions. Furthermore, as the model led us to expect, coefficient c_2 is mostly close to zero. The only two exceptions are the cases $V = 12$ for ML and $V = 12$ for RT, where c_2 has values of -0.12 and -0.15, respectively. In all other cases $|c_2|$ is smaller than about 0.06. Curves with $c_2 = 0$ represent the model-behavior exactly, so by setting $c_2 = 0$ for all the nine curves, we get three hypothetical observers corresponding closely in behavior to the real observers. Let us average per speed across these three hypothetical observers, so that they fuse into one. This results in the curves of the last panel in Fig. 5, the g_n-values of which are averages of the three g_n-values found per speed for the three subjects. It is interesting to compare performance of our real subjects with this hypothetical subject. To do so we scaled their data and replotted them as

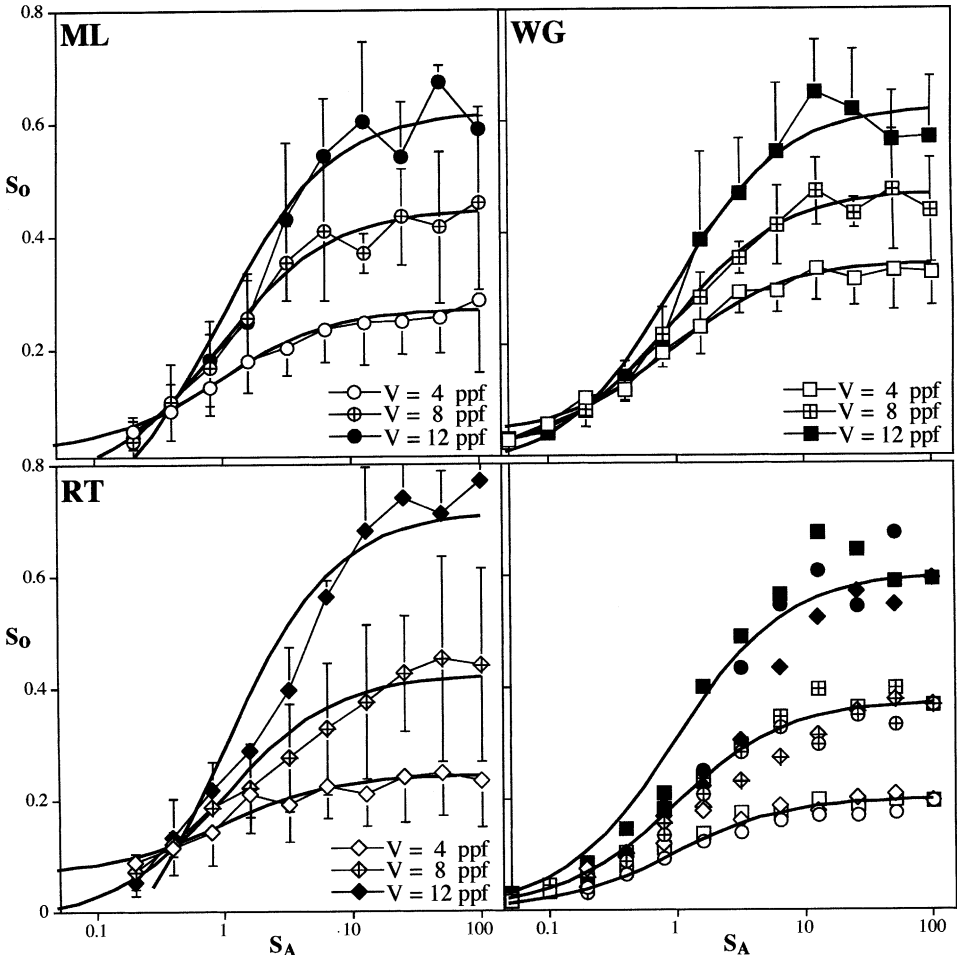

Fig. 5. Results of the second experiment. The first three panels present nulling threshold S_0 (ordinate) as a function of adaptation strength S_A (abscissa) for the three subjects ML (top left), WG (top right) and RT (bottom left). Each of these three panels presents data sets for three speeds, as indicated in the insets. The smooth curves are fitted functions, as given in formula (10) of the text. The fourth panel presents normalised data for the three subjects and three speeds, calculated as described in the text, compared to three curves representing the average of the model predictions for each speed. See the text for more details.

Table 2
Coefficient values c_2 and g_n of least-square fits of formula 10b to the psychophysical results of experiment 2 for three subjects and speeds (Fig. 5). The last column gives the correlation coefficients

Subject	Speed (ppf)	c_2	g_n	r^2
ML	4	0.019	4.98	0.987
	8	−0.038	9.64	0.980
	12	−0.120	14.7	0.958
WG	4	0.033	6.18	0.985
	8	0.002	9.32	0.991
	12	−0.028	12.94	0.977
RT	4	0.064	3.54	0.931
	8	−0.018	8.74	0.958
	12	−0.149	17.2	0.945

loose symbols in the last panel of Fig. 5. Data-scaling consisted of taking the ratio between S_0-values at maximum S_A for the hypothetical and the real observer and scale the data of the latter with this factor. It is clear from the result of this exercise that the hypothetical observer, behaving strictly according to the model's prescription, is an excellent representative of our three real observers, save for some linear scaling factor.

Table 2 shows that g_n, the noise gain, increases with speed and varies from a minimum of about 3.5 at 4 ppf (subject RT) to a maximum of about 17.5 at 12 ppf (same subject). This is a nice result, showing how dynamic noise is more effective in evoking a MAE at higher speeds.

In conclusion, the results of experiment 2, like those of experiment 1, provide strong support for the gain-control model and this time for mapping postulate (8b).

4.1.3. Experiment 3: speed-dependence of dMAE-duration, nulling threshold and their relation

From (7) and (8), the translation of x_0/x_t^0 into $g_m S_0/g_n$ as explained in the introduction to experiment 2, $S_0 = wg_n$ (see formula 10 for large S_A), and formula (4) with (8c) we have

$$T = 2.3\tau \,\mathrm{Log}[(g_m S_0 - w\theta)/\{\theta(1+S_0)^2\}] \quad (11a)$$

neglecting the small term $w\theta$ this gives

$$T/(2.3\tau) = \mathrm{Log}(g_m/\theta) + \mathrm{Log}\{S_0/(1+S_0)^2\} \quad (11b)$$

With this formula we can determine $\mathrm{Log}(g_m/\theta)$ as a function of speed, provided we know τ and measure T, and S_0 as a function of speed. For the purposes of this paper we will use rough estimates of τ as a function of V, derived from experiment 1. If we could somehow determine threshold θ from a separate psychophysical threshold measurement, it would become possible to calculate all model parameters (g_n from 10, g_m/θ from 11, θ from a relation to S_d). We will use the direction discrimination threshold value S_d for this purpose. In a separate analysis below we will then attempt to couple θ to S_d.

In the third experiment we therefore measured T, S_0, and S_d as a function of speed V, and used the data to estimate how the model variables change with speed. Fig. 6 presents the results of this experiment, in which speeds were used from 1–24 ppf (1.5–36 deg/s). The same three subjects participated as in the previous experiments. For each subject duration measures were repeated six times for every condition, whereas S_0 and S_d were measured three or four times per condition.

Fig. 6 also presents the ratio S_0/S_d, which was calculated to test a suggestion from previous work (van de Grind, Lankheet, van Hof, & Verstraten, 2000), that this ratio is a predictor of T-values. For two subjects (ML and WG) we indeed see that the ratio S_0/S_d is numerically approximately equal to T in a limited range of speeds. For the third subject this is not the case, however. The third subject in Fig. 6 (RT, bottom left), had higher direction discrimination thresholds (S_d-values) than the other subjects. This is the main reason why her S_0/S_d ratio's always fall short of being numerically equal to the MAE-duration in seconds. It was noticed during the experiments that nulling becomes more and more

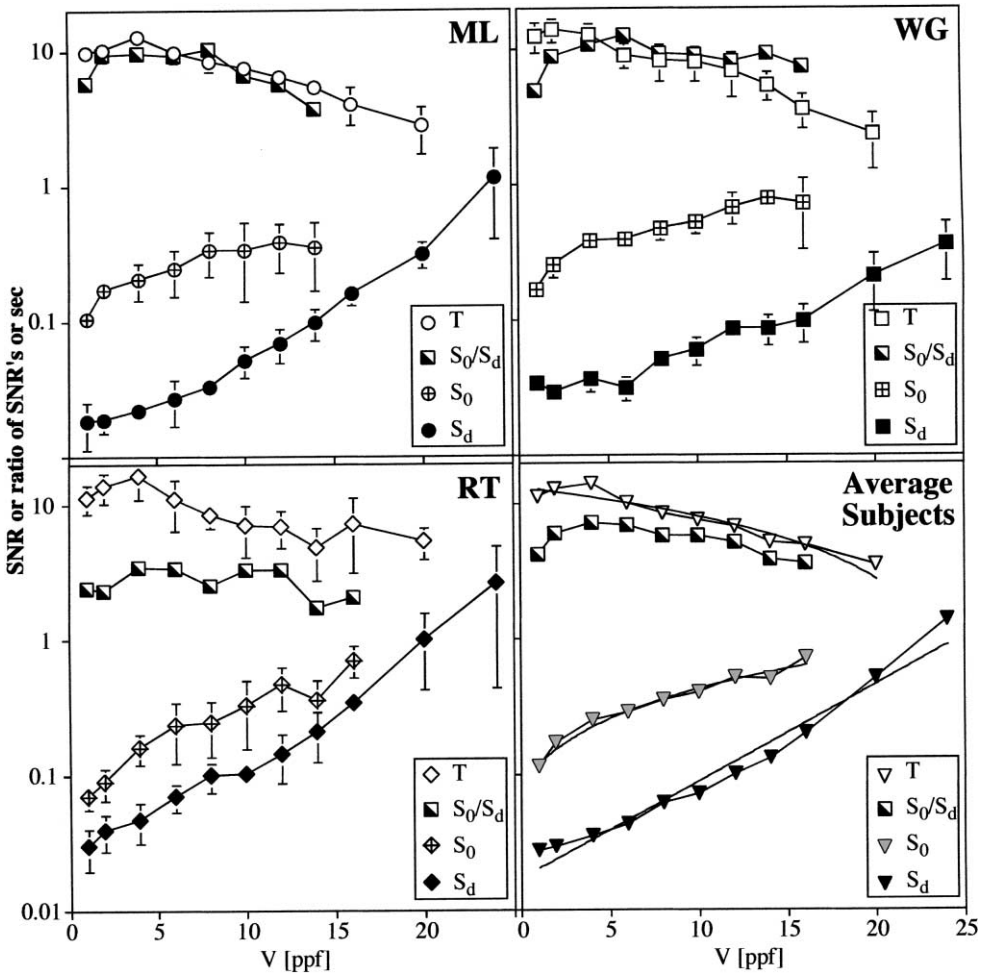

Fig. 6. Results of experiment 3. S_0 and S_d were measured three times for ML and RT and 4 times for WG, whereas T was measured six times for all subjects. Standard deviations are indicated by vertical bars, except where they are smaller than the symbol-size. Closed symbols: S_d-values, open symbols: MAE-durations T, crossed (or grey) symbols: nulling thresholds. Diagonally divided black–white square symbols represent the ratio S_0/S_d. The fourth panel presents averages for each speed across observers and the best fitting smooth functions through these points.

difficult for higher speeds, because it is difficult to clearly see the motion-direction at high speeds. Motion and its orientation (e.g. horizontal) are clearly seen, but the direction (e.g. left versus right) is uncertain. Thus the subjects often indicate 'wrong' directions, both when the MAE dominates and when the nulling stimulus dominates the balance between the two. This perceptual uncertainty increases the variance of the settings. Subjects then often felt the task became virtually impossible. That is why no nulling thresholds were obtained for some of the higher speeds. The direction discrimination performance deteriorated less for increasing speeds, and could be quantified up to 24 ppf (36 deg/s) and sometimes even up to 40 ppf (not shown).

For the speed-range of Fig. 6 we find a monotonously increasing direction-discrimination threshold S_d. An exponential function of the form $S_d = \alpha \times 10^{\beta}$ proved to give an good fit. The nulling threshold can be described by a linear increase with speed V over the measured range in Fig. 6. These regularities hold for all three subjects. The bottom right panel in Fig. 6 presents an average across subjects for all the data sets in the other three panels. Best fitting smooth functions are included in the figure. They are: $S_d = 0.02 \times 10^{0.057V}$ ($r^2 = 0.984$, V in ppf); $S_0 = 0.086 + 0.034V$ ($r^2 = 0.954$, V in ppf); $T = 13.34 - 0.558V$ ($r^2 = 0.862$, V in ppf). It should be emphasized that the model does not predict how T, S_0, and S_d change with speed V, making these curve fitting results irrelevant to the model. They are only intended as summaries of the psychophysical findings.

To calculate the model parameters from the psychophysical data we first need an estimate of τ as a function of speed. To this end we averaged the τ-values of Table 1 per speed across subjects, and fitted a linear relation to the resulting τ-values for the three speeds. This leads to $\tau(V) = 1.8 + 0.1\ V$ (s). With this rough estimate and formula (11b) we can, for every speed in the measured range, calculate g_m/θ, a 'threshold-normalised' motion gain, from the measured T and S_0-values. We used the average data of the fourth panel of Fig. 6 in this calculation. Because we know from formula (10) that for large S_A and long enough adaptation $S_0 = w \times g_n$, the noise gain factor g_n can be calculated from S_0. If we can determine θ from S_d we therefore have all the model parameters as a function of speed. This is an independent challenge, because it means coupling a MAE-model parameter (θ or g_m) to a normal unadapted motion system threshold parameter. This and the determination of all model parameters is the purpose of the following analysis.

4.2. Linking motion detection thresholds to MAE model-parameters

In the model description we stated that $x_d = \theta$, so it is tempting to translate x_d as $g_m S_d/(1 + S_d)$ and thus conclude that only the ratio of θ and g_m can be calculated from S_d. It is clear, however, that this would be a wrong assumption, because it would mean that the threshold is not influenced by the added noise, only by the motion signal. Noise gain g_n must also play a role. We will therefore assume that the noise component $g_n S_d^{-1}/(1 + S_d^{-1})$ increases the detection threshold. Actually there is no logical necessity to assume that this detection or discrimination threshold is the same as threshold θ that we used for MAE detection. Yet, in a model it is attractive to assume that it is, so that the number of degrees of freedom is as limited as possible. The assumption can be written as

$$g_m S_d/(1 + S_d) = \theta + g_n S_d^{-1}/(1 + S_d^{-1}) \quad (12a)$$

This detection postulate can be translated in a form containing the ratio g_m/θ, which we determined from the MAE-data (see above). The result is

$$\theta = g_n/\{S_d(g_m/\theta - 1) - 1\} \quad (12b)$$

We calculated θ with (12b) from S_d and the MAE data, then multiplied g_m/θ, as determined from the MAE-data alone, by this value of θ to obtain g_m. Fig. 7 shows the results of this analysis, θ, g_m and g_n as functions of V.

Provided the above coupling of θ to S_d is correct we can conclude from Fig. 7 that the motion gain g_m decreases slightly with increasing speed, that the noise gain g_n increases noticeably with speed and the threshold criterion θ even more, possibly to cope with the in-

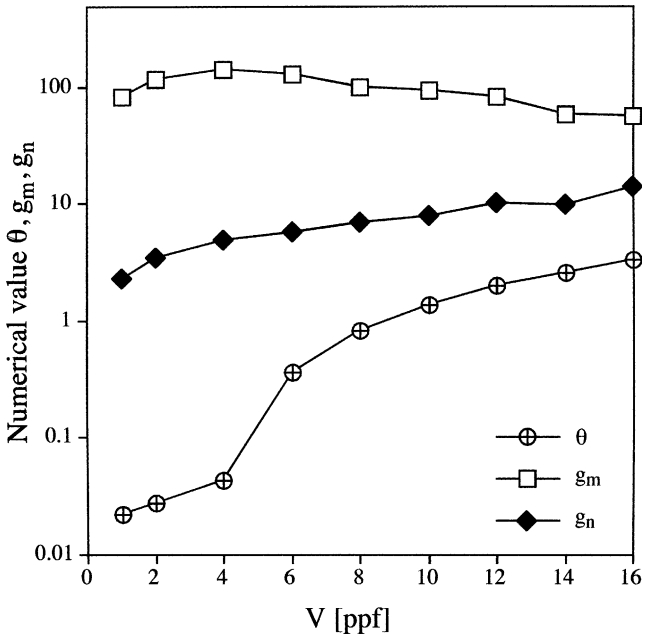

Fig. 7. Motion signal gain g_m, noise signal gain g_n, and threshold θ of the model, calculated with the model's formulae from psychophysical data of the fourth panel in Fig. 6. The calculation is described in the text. If these parameters are inserted in a model simulation we reproduce the data of Fig. 6 fourth panel, showing that the (approximation) formulae are satisfactory for the purposes of this paper.

creasing noise sensitivity. The high motion gain can easily be interpreted as a high convergence of motion sensors on each single gain-control unit. During strong-signal adaptation, g_m should preferably not exceed the value 10, because otherwise the input signal exceeds the range limits of the model. This is not a serious problem and it can be resolved without additional assumptions. The factor w, which we fixed from the start at a value of 0.05, can be varied to fine-tune the relation between direction discrimination threshold and MAE-data. This is easiest explained by solving formula (12b) for S_d:

$$S_d = (g_n/\theta + 1)/(g_m/\theta - 1) \quad (12c)$$

In most of the parameter ranges of this study we can neglect 1 relative to g_n/θ or g_m/θ, so that (12c) shows that $S_d \approx g_n/g_m$ and with $S_0 = wg_n$ we then find:

$$S_0/S_d \approx wg_m \quad (13)$$

This relation makes perfect sense, because it says that the ratio of a MAE-quantity (S_0) and the discrimination threshold is determined by how much signal one shunts via weight w into the adaptation pathway. The higher w, the higher the ratio between nulling and discrimination threshold. As a result we can shift the balance between adaptation effects and threshold values with w. If we increase w by some factor the calculated gain factors g_m and g_n go down by this factor. Since a calculation of the ratio g_m/θ from formula (11) is independent of this we still get the same MAE-duration if we also decrease θ by the same factor. Such a scale change does not influence the overall pattern of results in Fig. 7, only the numbers along the ordinate.

It is not trivial to link psychophysical detection or discrimination data to neuronal activity (Hol & Treue, 2001), let alone to a model mimicking neuronal activity at a more abstract level. Therefore, formula (12) should be viewed as a preliminary linking proposition. Its major strength is that it works in the context of the present model, but it is certainly desirable to design psychophysical experiments to test it more directly. This must be left to future work.

Because we used several approximations in deriving the formulae, an overall check of the above exposition by simulation of the model seemed necessary. We therefore simulated the model in Matlab 5.2, using Simulink, on a Macintosh G4. The simulation consists of wiring the various building blocks of Simulink in the appropriate way (similar to Fig. 3) and running a system simulation separately for each of the parameter choices. Results of our simulations confirmed the above reasoning and formulae. It was possible to reproduce all of the psychophysical data with a good accuracy by using the parameter values calculated as explained above. For $w = 0.05$ the simulation results were mostly less than $\pm 5\%$ different from the psychophysical data, except at the highest speeds of 21 and 24 deg/s, where the simulated values of S_0 differed 12% and 25% respectively from the psychophysical measures. A similar good fit was obtained for $w = 0.5$ if the model parameters were calculated with more exact formulae. (The handy approximations above were mostly based on the assumption that the term $w\theta$ is small and can be neglected.) Taken together the model-simulation data and psychophysical data were in excellent agreement.

In summary: The psychophysical results of experiment 3 suggest that nulling thresholds increase and MAE-durations decrease about linearly in the medium-to-high speed range, while direction discrimination thresholds increase exponentially with speed. When we use the psychophysical findings to estimate model and mapping parameters we find that the noise gain is linearly proportional to S_0 (formula (10), experiment 2), and thus (like S_0) increases about linearly with V. The model's threshold θ increases with speed, slowly at medium speeds and faster at higher speeds (Fig. 7). The motion gain decreases modestly with speed (Fig. 7).

5. Discussion

The three experiments and accompanying data analysis of this paper show that it is possible in principle to fit the model to empirical data and this was illustrated with quantitative fits. Of course, this is only a proof of the principle. More experiments are needed to quantitatively fit the model to psychophysical data. Notably, it would be useful to develop a more direct way to determine psychophysically how θ relates to S_d. Also the data on time constant τ are somewhat meager at this time. Yet, we think we have shown conclusively that a gain-control model as developed above can indeed couple MAE-duration and nulling data, and that it is possible to determine the model parameters from psychophysical experiments. The correspondence between model predictions and psychophysical findings in the first two experiments was impressive enough to accept the presented gain-control model as a tool of thought in designing and describing experiments on the dMAE. The third experiment showed how one can, in a practical case—the study of speed-dependence—tune the model to psychophysical results. This led to sensible results, and thus gives us some confidence in assuming that the model might be a valuable tool to design new experiments and interpret the results. Also support for formula (8) which maps the psychophysical domain on the model domain, proved to be strong. Experiments 1 and 2, fully confirm the expectations derived from the model analysis, including formula (8). We think our gain-control model provides a promising start of an attempt to develop models explaining both motion detection and motion aftereffects in a single model. However, our model only holds for one of the motion systems, as argued below.

After a sufficiently long adaptation to a moving RPA (or sparser random-dot pattern) one can evoke a sMAE by testing with a static pattern of similar spatial structure as the adaptation pattern. If one tests with dynamic noise, however, a MAE is found with different properties (Blake & Hiris, 1993; Hiris & Blake, 1992), the dMAE. The sMAE can only be experienced for relatively low adaptation speeds, below about 12–20 deg/s, whereas the dMAE can be generated by medium- to high-speed adaptation patterns of up to 40–80 deg/s in the fovea (Verstraten, van der Smagt, & van de Grind, 1998, 1999). Conversely, at the lowest speeds one can only evoke a sMAE, no dMAE (Verstraten et al., 1998, 1999). The different properties of the relatively low-speed (*s*-) and relatively high-speed (*d*-) MAE have been extensively documented in our laboratory (van de Grind et al., 2001; van der Smagt et al., 1999; Verstraten et al., 1998, 1999). In this paper we used an LSNR-nulling method and thus we always had noise in the compensation stimulus while setting the nulling-threshold. Therefore what we compensated (cancelled, nulled) must always have been the dMAE. As a consequence, all results and conclusions in this paper are only directly valid for the dMAE. To the extent that a similar gain-control model also holds for the sMAE, nulling of the sMAE is not made impossible by the fact that it requires compensation of a 'paradoxical' motion experience with real motion. The paradoxical aspect of the classical MAE probably stems from simultaneous activation of both the slow motion system and a position analysis system by a static test stimulus. This leads to the percept of a static pattern, the details of which have a fixed position, and motion at the same time and place. Dynamic noise, as used for the dMAE, does not seem to stimulate any local position detectors, so that no paradoxical experience of fixed position and motion arises. Empirical support for this interpretation has been presented elsewhere (Fig. 1 in van de Grind et al., 2001).

A question that arises from this reasoning is whether a similar cancellation method would be possible for the sMAE evoked by coherently moving RPAs. At first sight, the literature appears to be replete with successful nulling methods for the sMAE (e.g. Bex, Metha, & Makous, 1999; Chichilnisky, Heeger, & Wandell, 1993; Cords & von Brücke, 1907; Culham, Verstraten, Ashida, & Cavanagh, 2000; Gregory, 1985; Harris, Morgan, & Still, 1981; Johnston & Wright, 1983; Ledgeway, 1994; McCarthy, 1993; Murakami, 1995; Murakami & Shimojo, 1995; Pantle, 1978; Sachtler & Zaidi, 1993; von Grünau & Dubé, 1992; Wright, 1986; Wright & Johnston, 1985). However, it is by no means certain that all these studies probed the sMAE. As we will see below, a counterphasing test (and nulling) pattern is likely to evoke the so-called counterphase-flicker-MAE or cMAE. Indeed, all these studies used periodic patterns such as sinewaves. The spatial properties of these patterns are described by a one-dimensional discrete Fourier-spectrum. Pairs of identical patterns of this kind, moving in opposite directions at equal speed make up a static counterphase-flickering pattern. The idea is that such a pattern provides equal stimulation to opponent motion detectors perpendicular to the grating bars. For vertical grating bars, motion sensors tuned to motion to the left and to the right are equally activated, unless one has adapted to motion to the right, say. In that case one sees motion to the left, because the rightward sensors are desensitised. By decreasing contrast of the leftward component of the counterphasing test pattern, the MAE can then be nulled. The problem is that one combines static position information (as is necessary to evoke a sMAE) and flicker in this test stimulus. It appears likely that flicker stimulates motion sensors driven by transient input cells, that do not play a role in the classical sMAE. Therefore the MAE measured by this nulling technique might be the sum of a sMAE and a flicker-selective MAE. As we will see below this is not just an academic worry. The cMAE has properties that differ from those of the sMAE (e.g. Ashida & Osaka, 1994; Nishida & Sato, 1995). Whereas an opponent pair of sinewave gratings with equal parameters completely cancel each others motion, no such cancellation occurs for opponently moving RPAs. On the contrary, one can see them move transparently across each other and they do not cancel each others motion information at all. They do decrease each others visibility or detectability, but this effect is rather modest (Lindsey & Todd, 1998). In a pilot study with three observers, we attempted to null the sMAE evoked by a moving RPA with real motion of the test RPA, which was of variable contrast. This proved to be impossible. As soon as the test pattern became visible (differed visibly from a uniform field) it was seen in transparent motion with the sMAE. In itself this observation of transparency of a sMAE and a (test) motion stimulus is interesting, but it disqualifies the nulling method in this domain. It was just as impossible to null a sMAE for moving RPAs by changing the speed of the test pattern rather than contrast.

This finding warns us against the assumption that counterphase-flicker MAEs of the moving sinewave literature are identical to what we call dMAEs in this paper. Discovery of the cMAE was preceded by the discovery of an other 'flicker'-MAE by Green, Chilcoat, and Stromeyer (1983). This flicker MAE was seen on spatially homogeneous flickering test fields, and showed no interocular transfer. The cMAE on the other hand shows interocular transfer and differs also in other respects from the flicker-MAE of Green et al. (Nishida & Sato, 1995). Interestingly the Green et al. stimulus hardly contains position information, whereas the cMAE might require both static position and flicker signals, as argued above. Second-order motion does not lead to a sMAE, but does evoke a MAE on dynamic test patterns

(Ledgeway, 1994; McCarthy, 1993), such as counterphase flickering patterns (von Grünau & Dubé, 1992). The cMAE is strong for high temporal and low spatial frequencies (like the dMAE), whereas the sMAE is strong for relatively low temporal frequencies. Thus there are parallels between the dichotomy sMAE versus cMAE for sinewaves on the one hand, and the dichotomy sMAE versus dMAE for moving RPAs on the other hand. Yet these dichotomies are not identical. If one uses a counterphasing RPA test, in analogy with the counterphasing sinewave tests, the resulting MAE evoked by adaptation to moving RPAs has properties in between our sMAE and dMAE (van der Smagt, 1999, chapter 5; van der Smagt, Verstraten, & van de Grind, 2000). Such a cMAE for RPAs has longer duration for low speeds than the dMAE, but shorter than the sMAE, whereas it has longer durations than the sMAE but shorter than the dMAE at higher speeds. It appears to be a mixture of responses from the low-speed and high-speed channel that are read out in isolation by a static RPA or dynamic noise, respectively (van de Grind et al., 2001; van der Smagt et al., 1999). We conclude from this that our present nulling-method exclusively addresses what we have called a high-speed motion channel, and that the above model, relating MAE-duration to the nulling LSNR-threshold, should be evaluated in this restricted context. It is not unlikely that a similar model can be formulated for the sMAE evoked by moving RPAs (low-speed channel) and evaluated with a suitable noise-free and flicker-free nulling method. This remains to be explored, but a suitable nulling method has not yet been found for the sMAE of RPAs.

Despite this lack of a full-blown model for the sMAE, one can at least check some of the above ideas. For example, Keck, Palella, and Pantle (1976) studied sMAE-duration as a function of contrast for sinewave gratings. Formula (9a) of our model appears to describe their results well if S_A in the formula is replaced by C, the contrast of the sinewaves. Results in their Fig. 1 are described quite well by this formula, e.g. their data for the test contrast of 1.7% could be described by $T = 18.7 + 35.3\,\mathrm{Log}\{C/(1+C)\}$, with $r^2 = 0.98$. If this can be interpreted as in our model, it would signify a time constant of 15 s (35.3/2.3) for their sMAE. This example suggests that the model of this paper might also help in understanding some of the sMAE findings. Moreover, Nishida, Ashida, and Sato (1997) showed that there was little difference between the contrast dependence of the sMAE and cMAE. Therefore the validity of the model ideas might also extend to the cMAE. Yet, one must keep in mind that this requires a number of important changes in the model. A noise test is ineffective for the sMAE, whereas a static test is. Therefore, the noise action of our model, which extends to all direction-tuned channels, should be replaced by an input from static stimuli (such an input was already suggested by Keck et al., 1976). It is not immediately obvious how this should be done to comply with the finding that a lower contrast test gives a longer duration for the sMAE. It would also be necessary to rethink the implementation of nulling, and solve the riddle why it is so difficult to null an sMAE evoked and tested with RPAs.

We presented a gain-control model that can be inserted in the Grunewald-network model of the introduction and showed that it predicts a simple relation between dMAE-duration T and adaptation strength, as well as between the nulling threshold S_0 and adaptation strength. The data confirm the predictions. We showed that MAE-durations and nulling-thresholds provide similar information on the underlying mechanisms. Thus, there is no urgent need any more to measure dMAE-durations, with the inherently large variance and low repeatability, because one can use more robust nulling data instead. Usually some form of gain-control has been presumed to be responsible for the MAE, yet there is a lack of explicit gain-control models in the MAE-literature. Similarly, recovery from adaptation has often been described by a negative exponential function. But, these descriptions have mostly been verbal rather than in the form of a simulation or a mathematical model. One exception is the work by Sachtler and Zaidi (1993) who formulated a feedforward multiplicative gain-control model like the one we called an FFM-control above. However, they did not need to explicitly specify the dynamic properties of their model, because they used it to explain equilibrium data. Thus a direct comparison is not possible, but a version of their gain control, as used in some of our simulation studies, might work just as well as the model we analysed in depth in this paper. Like Sachtler and Zaidi (1993) we found it advantageous to formulate the gain-control model in sufficient detail to guide us in interpreting psychophysical findings.

There is an additional advantage to the use of this type of explicit model of a gain-control stage. With reference to Fig. 2 it is clear that the gain controls could get additional input from nearby channels, tuned to other orientations, speeds, spatial or temporal frequencies. This would mean that it is possible to null the MAE of speed V_1 or orientation α with a different speed V_2 or orientation β. Eventually these interactions will have to be specified in such a way that they describe results for bivectorial adaptation with different speeds (Verstraten et al., 1994) in some detail and explain the perceptual 'slowing down' of both the adaptation stimulus and the MAE with time. A mathematical description of such speed-interactions as given by Hammett, Thompson, and Bedingham (2000) might serve as a guide, even though their formulation cannot be completely correct. It disallows motion transparency for different speeds and neglects the transparent MAE for a combination of fast and slow motion adaptation (van der Smagt et al., 1999).

Thus formulating proper interactions in the speed domain is probably more complex than in the direction domain and must be left to future work. Similarly one can adapt to speed V_1 with a given frame rate and try to null with speed V_1 at a different frame rate. This will give insight into the temporal tuning range of the motion sensors and gain-controls in the model. Therefore an explicit model as presented in this paper is a useful tool of thought, suggesting sensible experiments that will allow a step by step refinement of the model and will thus deepen our insight into the relation between MAEs and the structure of our motion perception systems.

Acknowledgements

We thank Ans van Doorn and Richard van Wezel for discussions and insightful remarks on the manuscript. We are grateful for the hours Frans Verstraten, Maarten van der Smagt, and Paulion van Hof spent in our set-up during pilot experiments. Ran Tao held a visiting grant from the P.R. of China.

Appendix A

The analysis is done for two opponent channels of the network, one of which has been adapted. We consider the situation at time t during recovery, where $t = 0$ is the end of adaptation and start of testing. The adapted channel's leaky integrator then has a charge:

$$u_1 = u^* \exp(-t/\tau) + wx_t\{1 - \exp(-t/\tau)\}$$

Here the first term is the leak-term, which describes a decreasing influence of adaptation charge u^* with time during testing, and the second term represents the integrator's charging due to the test stimulus. They can be added according to the superposition principle for linear systems. For the non-adapted channel we call the corresponding leaky integrator variable u_2, and it has the same second term as u_1 above, but no first term (no adaptation charge). The MAE ends if the difference between the output of the non-adapted and adapted channel equals and becomes less than threshold criterion θ, so at $t = T$

$$x_t/(1 + u_2) - x_t/(1 + u_1) = \theta$$

To simplify the typography we now leave out the star from u^* and write x for x_t, call $\exp(-T/\tau) = E$ and $1 + wx = a$. This leads to

$$(a - wxE)(a - wxE + uE) = xuE/\theta \tag{A.1}$$

From this equation we want to solve E, because if $E^{-1} = Y$ we have the solution as $T = \tau \mathrm{Ln}(Y)$. Although an exact solution is possible the result is unwieldy, so we decided to work with reasonable approximations that emphasize the main factors. First of all we dropped all terms with E^2, because E is a very small number, and in the solution for E^{-1} we then also dropped a term $2wx\theta$, because it is small relative to the other terms. This led to

$$E^{-1} \approx u(x - a\theta)/(\theta a^2) = bu/\theta \tag{A.2}$$

with

$$b \approx (x - \theta)/(1 + wx)^2 \tag{A.3}$$

where we again dropped a term ($w\theta x$ relative to x). The above simplifications might not be valid for other choices of the parameters than we use in this paper, but one can always use the exact solution, if necessary. To gain a deeper insight in the model's behavior, the presented simplifications are very convenient, and deviations from the exact solution are mostly smaller than 5–10% for the parameter values used in this paper. Formula (A.2) gives formula (3) of the text and (A.3) gives formula (4) of the text, where the indices are of course restored.

References

Ashida, H., & Osaka, N. (1994). Difference of spatial frequency selectivity between static and flicker motion aftereffects. *Perception, 23*, 1313–1320.

Bex, P. J., Metha, A. B., & Makous, W. (1999). Enhanced motion aftereffect for complex motions. *Vision Research, 39*, 2229–2238.

Blake, R., & Hiris, E. (1993). Another means for measuring the motion aftereffect. *Vision Research, 33*, 1589–1592.

Chichilnisky, E.-J., Heeger, D., & Wandell, B. A. (1993). Functional segregation of color and motion perception examined in motion nulling. *Vision Research, 33*, 2113–2125.

Cords, R., & von Brücke, E. (1907). Über die Geschwindigkeit des Bewegungsnachbildes. *Archiv für die gesammelte Physiologie des Menschen und der Thiere, 119*, 54–76.

Culham, J. C., Verstraten, F. A. J., Ashida, H., & Cavanagh, P. (2000). Independent aftereffects of attention and motion. *Neuron, 28*, 607–615.

Green, M., Chilcoat, M., & Stromeyer, C. F. (1983). Rapid motion aftereffect seen within uniform test fields. *Nature, 304*, 61–62.

Gregory, R. L. (1985). Movement nulling: for heterochromatic photometry and isolating channels for 'real' and 'apparent' motion. *Perception, 14*, 193–196.

Grunewald, A. (1996). A model of transparent motion and non-transparent motion aftereffects. In D. S. Touretzky, M. C. Mozer, & M. E. Hasselmo (Eds.), *Advances in Neural Information Processing Systems* (*Vol. 8*, pp. 837–843). Massachusetts, USA: MIT Press Cambridge.

Grunewald, A., & Lankheet, M. J. M. (1996). Orthogonal motion after-effect illusion predicted by a model of cortical motion processing. *Nature, 384*(6607), 358–360.

Hammett, S. T., Thompson, P. G., & Bedingham, S. (2000). The dynamics of velocity adaptation in human vision. *Current Biology, 10*, 1123–1126.

Harris, L. R., Morgan, M. J., & Still, A. W. (1981). Moving and the motion aftereffect. *Nature, 293*, 139–141.

Hiris, E., & Blake, R. (1992). Another perspective on the visual motion aftereffect. *Proceedings of the National Academy of Sciences USA, 89*, 9025–9028.

Hol, K., & Treue, S. (2001). Different populations of neurons contribute to the detection and discrimination of visual motion. *Vision Research, 41*, 685–689.

Johnston, A., & Wright, M. J. (1983). Visual motion and cortical velocity. *Nature, 304*, 436–437.

Keck, M. J., Palella, T. D., & Pantle, A. (1976). Motion aftereffect as a function of the contrast of sinusoidal gratings. *Vision Research, 16*, 187–191.

Ledgeway, T. (1994). Adaptation to second-order motion results in a motion aftereffect for directionally-ambiguous test stimuli. *Vision Research, 34*, 2879–2889.

Lindsey, D. T., & Todd, J. T. (1998). Opponent motion interactions in the perception of transparent motion. *Perception & Psychophysics, 60*, 558–574.

Mather, G. (1980). The movement aftereffect and a distribution-shift model for coding the direction of visual movement. *Perception, 9*, 379–392.

Mather, G., & Harris, J. (1998). Theoretical models of the motion aftereffect. In G. Mather, F. Verstraten, & S. Anstis (Eds.), *The motion aftereffect. A modern perspective*. Cambridge, MA: Bradford Book, The MIT Press (Chapter 7).

McCarthy, J. E. (1993). Directional adaptation effects with contrast modulated stimuli. *Vision Research, 33*, 2653–2662.

Moulden, B., & Mather, G. (1978). In defence of a ratio model for movement detection at threshold. *Quarterly Journal of Experimental Psychology, 30*, 505–520.

Murakami, I. (1995). Motion aftereffect after monocular adaptation to filled-in motion at the blind spot. *Vision Research, 35*, 1041–1045.

Murakami, I., & Shimojo, S. (1995). Modulation of motion aftereffect by surround motion and its dependence on stimulus size and eccentricity. *Vision Research, 35*, 1835–1844.

Nishida, S., Ashida, H., & Sato, T. (1997). Contrast dependencies of two types of motion aftereffect. *Vision Research, 37*, 553–563.

Nishida, S., & Sato, T. (1995). Motion aftereffect with flickering test patterns reveals higher stages of motion processing. *Vision Research, 35*, 477–490.

Pantle, A. J. (1978). Temporal frequency response characteristic of motion channels measured with three different psychophysical techniques. *Perception & Psychophysics, 24*, 285–294.

Pantle, A. J. (1998). How do measures of the motion aftereffect measure up? In G. Mather, F. Verstraten, & S. Anstis (Eds.), *The motion aftereffect. A modern perspective*. Cambridge, MA: Bradford Book, The MIT Press (Chapter 2).

Raymond, J. E. (1993). Movement direction analysers: Independence and bandwidth. *Vision Research, 33*, 767–775.

Sachtler, W., & Zaidi, Q. (1993). Effect of spatial configuration on motion aftereffects. *Journal of the Optical Society of America A, 10*, 1433–1449.

Sutherland, N. S. (1961). Figural after-effects and apparent size. *Quarterly Journal of Experimental Psychology, 13*, 222–228.

van de Grind, W. A., Grüsser, O.-J., & Lunkenheimer, H.-U. (1973). Temporal transfer properties of the afferent visual system: Psychophysical, neurophysiological and theoretical investigations. In R. Jung (Ed.), *Handbook of sensory physiology, Vol. VII/3A (Central processing of visual information)* (pp. 431–573). Springer Verlag (Chapter 7).

van de Grind, W. A., Lankheet, M. J. M., van Hof, P., & Verstraten, F. A. J. (2000). How a motion-aftereffect compensation method can lead to a reliable prediction of motion aftereffect durations. *ARVO 2000, Investigative Ophthalmology & Visual Science, 41*(4), 4205.

van de Grind, W. A., van Hof, P., van der Smagt, M. J., & Verstraten, F. A. J. (2001). Slow and fast visual motion channels have independent binocular rivalry stages. *Proceedings of the Royal Society, London B, 268*, 437–443.

van der Smagt, M. J. (1999). Integration and segregation mechanisms in human motion vision. Ph.D. Thesis, Utrecht University. ISBN 90-393-2100-0.

van der Smagt, M. J., Verstraten, F. A. J., & van de Grind, W. A. (1999). New transparent motion aftereffect. *Nature Neuroscience, 2*, 595–596.

van der Smagt, M. J., Verstraten, F. A. J., & van de Grind, W. A. (2000). Do motion aftereffects depend on test-pattern temporal frequency? *Perception, 28c*(suppl).

van Doorn, A. J., & Koenderink, J. J. (1982a). Temporal properties of the visual detectability of moving spatial white noise. *Experimental Brain Research, 45*, 179–188.

van Doorn, A. J., & Koenderink, J. J. (1982b). Spatial properties of the visual detectability of moving spatial white noise. *Experimental Brain Research, 45*, 189–195.

von Grünau, M. W., & Dubé, S. (1992). Comparing local and remote motion aftereffects. *Spatial Vision, 6*, 303–314.

Verstraten, F. A. J. (1996). On the *ancient* history of the direction of the motion aftereffect. *Perception, 25*, 1177–1187.

Verstraten, F. A. J., Fredericksen, R. E., & van de Grind, W. A. (1994). Movement aftereffect of bi-vectorial transparent motion. *Vision Research, 34*, 349–358.

Verstraten, F. A. J., van der Smagt, M. J., & van de Grind, W. A. (1998). Aftereffect of high-speed motion. *Perception, 27*, 1055–1066.

Verstraten, F. A. J., van der Smagt, M. J., Fredericksen, R. E., & van de Grind, W. A. (1999). Integration after adaptation to transparent motion: static and dynamic test patterns result in different aftereffect directions. *Vision Research, 39*, 803–810.

Wade, N. J. (1994). A selective history of the study of visual motion aftereffects. *Perception, 23*, 1111–1134.

Wade, N. J. (1998). *A natural history of vision*. Cambridge, MA: Bradford Book. The MIT Press.

Watson, A. B., & Pelli, D. G. (1983). Quest: a Bayesian adaptive psychometric method. *Perception & Psychophysics, 33*, 113–120.

Wright, M. J. (1986). Apparent velocity of motion aftereffects in central and peripheral vision. *Perception, 15*, 603–612.

Wright, M. J., & Johnston, A. (1985). Invariant tuning of motion aftereffect. *Vision Research, 25*, 1947–1955.